electronics

MDPI

Article

The Joint Estimation of SOC-SOH for Lithium-Ion Batteries Based on BiLSTM-SA

Lingling Wu, Chao Chen *, Zhenhua Li, Zhuo Chen and Hao Li

College of Computer Science and Engineering, Sichuan University of Science and Engineering, Zigong 643000, China; 323085406126@stu.suse.edu.cn (L.W.); 322085406210@stu.suse.edu.cn (Z.L.); 323085406203@stu.suse.edu.cn (Z.C.); 323085406210@stu.suse.edu.cn (H.L.)

* Correspondence: chenchao@suse.edu.cn

Abstract: Lithium-ion batteries are commonly employed in energy storage because of their extended service life and high energy density. This trend has coincided with the rapid growth of renewable energy and electric automobiles. However, as usage cycles increase, their effectiveness diminishes over time, which can undermine both the system's performance and security. Therefore, monitoring the state of charge (SOC) and state of health (SOH) of batteries in real time is particularly important. Traditional SOC calculation methods typically treat SOC and SOH as independent variables, overlooking the coupling between them. To tackle this issue, the paper introduces a joint SOC-SOH estimation approach (BiLSTM-SA) that leverages a bidirectional long short-term memory (BiLSTM) network combined with a self-attention (SA) mechanism. The proposed approach is validated using a publicly available dataset. With the SOH taken into account, the MAE and RMSE of the SOC are 0.84% and 1.20%, showing notable increases in accuracy relative to conventional methods. Additionally, it demonstrates strong robustness and generalization across datasets with multiple temperatures.

Keywords: SOC estimation; SOH estimation; lithium-ion battery; BiLSTM; SA

Academic Editors: Krzysztof Górecki, Paweł Górecki and Kalina Detka

Received: 27 November 2024
Revised: 23 December 2024
Accepted: 26 December 2024
Published: 29 December 2024

Citation: Wu, L.; Chen, C.; Li, Z.; Chen, Z.; Li, H. The Joint Estimation of SOC-SOH for Lithium-Ion Batteries Based on BiLSTM-SA. *Electronics* **2025**, *14*, 97. https://doi.org/10.3390/electronics14010097

1. Introduction

In the current clean and efficient energy sector, lithium-ion batteries are becoming increasingly important due to their superior energy density and extended service life [1]. This trend has coincided with the rapid growth of renewable energy and electric automobiles. Lithium-ion batteries are a key element in systems for storing energy, and they degrade with increasing usage cycles in practical applications. Their performance and lifespan directly affect the reliability of batteries and the safety of the system, leading to reduced system performance and potential safety risks during operation [2]. Therefore, the accurate monitoring and management of the operating state of it are crucial to ensuring its safety, reliability, and efficient performance. The state of charge (SOC) and the state of health (SOH) are critical variables that define the operational state of a battery [3]. SOC stands for the present capacity as a percentage of its maximum capacity, directly correlating to its immediate performance. SOH represents the degree of a battery's aging compared to a new one, directly influencing its long-term performance and service life [4].

Reliable SOC and SOH estimation is a fundamental component of the battery management system (BMS), as the preciseness of their estimation immediately impacts the security, effectiveness, and lifespan of the battery and helps to precisely gauge the remaining driving range of the vehicle, providing drivers with reliable range information [5]. Although several approaches have been employed to forecast SOC and SOH, current BMSs still have

a difficult time handling the intricacies of battery decline. In particular, as the battery ages, changes in SOH have an impact on how accurately SOC is estimated. As the number of lithium battery cycles increases, SOH gradually decreases, and the battery's maximum usable capacity changes. Both of these elements affect how accurate SOC estimation is. In addition to improving SOC estimation accuracy, precise SOH estimation enables the early identification of battery cells with significant capacity degradation, preventing performance loss or safety risks caused by uneven aging [6,7]. Therefore, considering the effect of SOH on SOC is crucial when estimating SOC. By jointly estimating both SOC and SOH, we can not only improve SOC estimation accuracy but also reduce performance degradation and mitigate potential safety hazards. With electric vehicles, this is particularly important, where the timely replacement of severely degraded batteries can prevent traffic accidents caused by battery failures, thereby safeguarding vehicle safety and reliability [8]. Estimating SOC and SOH together is significant so as to optimize BMS performance, improve battery efficiency, and enhance user safety. It not only contributes to better battery performance but also directly impacts the vehicle's safe operation and the overall driving experience.

Traditional SOC estimation methodologies fall into three main categories: model-based [9], open-circuit voltage (OCV) [10], and Coulomb counting methods [11]. Coulomb counting forecasts SOC by tracking the charging and discharging currents of the battery, as well as its total charge. However, due to factors like battery self-discharge, sensor inaccuracies, and temperature fluctuations, this method is susceptible to cumulative errors, which can progressively increase, particularly during long-term use [12]. Through voltage measurement of the battery, the OCV method calculates SOC under static conditions. However, it needs the battery to remain idle for a while without load to allow voltage stabilization, which limits its practical applicability. The complexity and high computational demands of model-based methods also restrict their use in real-time, online applications [13]. The two main categories of traditional methods to estimate SOH are direct calculation and model-based methods [14]. Direct calculation approaches often require stringent experimental and hardware conditions, making them inappropriate for online real-time monitoring. Approaches based on models, on the other hand, typically involve complex model parameter fitting and require a significant quantity of experimental data, which increases both the cost and the difficulty of their implementation [15].

Data-driven methods have garnered major attention in SOC and SOH estimation due to the considerable variation in parameters across different battery types under diverse conditions, which complicates the identification of numerous parameters in battery models [16,17]. In the context of a data-driven methodology, advanced computational approaches like machine learning and deep learning are employed. These approaches can be used to detect and analyze complex nonlinear relationships in batteries [18]. Their key advantage is their capacity to adjust to changes in battery characteristics, which enhances the precision and robustness of SOC and SOH estimation and demonstrates greater adaptability in practical applications. Especially when handling complex working conditions, data-driven methods can effectively adapt to changing environments and usage scenarios, demonstrating strong robustness and adaptability. In contrast to traditional methodologies, these data-driven techniques do not depend on complex model architectures or exact physical equations. Rather, they utilize models developed through training on extensive datasets, enabling them to provide highly precise estimations. Models like support vector machines, XGBoost, and neural networks have been used extensively for SOC and SOH estimation [19–22]. Bian et al. [23] introduced a stacked BiLSTM model, which exhibited remarkable accuracy in estimating the SOC across diverse ambient temperature scenarios. Eddahech et al. [24] used FNN for SOC estimation, and their results enabled the estima-

tion of the battery's end voltage. Yang et al. [25] used a recursive neural network for SOC estimation, achieving good accuracy when validated under dynamic load conditions. Zhang et al. [26] showed good accuracy under dynamic load conditions by estimating SOC under complex conditions using a traditional BP neural network. Zhong et al. [27] suggested a recursive neural network estimation method using the Kalman filter, achieving lightweight SOC estimation. Park et al. [28] applied wavelet transforms in combination with long short-term memory (LSTM) to estimate SOH using LSTM in combination with CNN. Qian et al. [29] pitched a multi-source Seq2Seq model for the accurate long-term prediction of lithium-ion SOH when loaded dynamically. Yang et al. [30] put forward a SOC estimation method via bidirectional LSTM networks improved by the Bayesian optimization algorithm. Van et al. [31] put forward a methodology for estimating SOH and internal resistance that makes use of LSTM networks.

However, the connection between SOC and SOH is ignored by most SOC and SOH estimation techniques in the aforementioned research. In actuality, the decrease in SOH that comes with lithium-ion battery aging and extended use inevitably impacts how precise SOC estimation is. SOC and SOH are interdependent, influencing each other dynamically. To address these limitations, a joint estimation approach is proposed. The combined SOC-SOH estimation method accounts for the intricate connection between SOC and SOH and adapts to changes in the battery's health condition to produce more precise SOC and SOH forecasts. Therefore, it is important to effectively integrate the time-scale characteristics of SOC and SOH, as well as their coupling relationship, in the estimation process. For real-time parameter updating and identification within an equivalent circuit model, Lai et al. [32] introduced a joint SOH-SOC strategy that uses the FFRLS. However, it is highly reliant on the model's precision, which limits its ability to fully achieve real-time SOC estimation. The enhanced firefly algorithm-optimized particle filtering technique for joint SOC and SOH estimation was presented via Wu et al. [33] using a second-order RC equivalent circuit model (2RCECM) and RLS for battery parameter recognition. However, the battery's complex nonlinear characteristics might not be adequately captured by the 2RCECM, which may limit the model's adaptability under various operating circumstances. Fang et al. [34] proposed a distributed optimal Kalman consensus filter for SOC and SOH estimation. Nevertheless, it does not adequately account for the various uncertainties and complexities encountered in practical applications, which limit the broader applicability of the results.

With the aim of resolving the issues mentioned above, this paper proposes an approach to the joint estimation of SOC-SOH, BiLSTM-SA, which incorporates bidirectional long short-term memory (BiLSTM) network with the self-attention mechanism (SA). BiLSTM-SA utilizes data from multiple cycles to capture the long-term decay characteristics of the battery so as to perform SOH estimation. It then combines the long-term information of the SOH estimation to achieve SOC estimation on the input features based on each discharge cycle, which not only effectively utilizes the influence of SOH changing capacity of the battery but also ensures the real-time nature and accuracy of the SOC estimation. Furthermore, the joint estimation of SOC-SOH is validated on a dataset containing multiple temperatures and different operating conditions, which fully considers the battery's performance fluctuations across various environmental conditions. This ensures that the model can adapt to the various challenges the battery may encounter in real-world use, such as extreme temperatures, rapid charging and discharging, and load variations, thereby increasing its ability for generalization and robustness. Therefore, the proposed BiLSTM-SA enhances both the model's estimation precision and its reliability in practical applications. The following are the contributions made by this paper:

1. The introduction of a segmented training strategy and the realization of joint SOC and SOH estimation through shared parameters effectively capture the interdependence between these two state variables, while reducing model complexity.
2. An estimation model is designed using BiLSTM to capture the bidirectional dependencies in battery time series data. The model's estimation accuracy for SOC and SOH is significantly improved by highlighting the key local features through the SA.
3. Addressing the differences in time scales between SOH and SOC, the proposed estimation strategy combines the short-term dynamic behavior and lengthy decay characteristics of the battery, focusing on real-time state estimation within each discharge cycle. This approach effectively adapts to changes in different time scales and boosts both the preciseness and timeliness of the estimation.

2. Materials and Methods

2.1. Bidirectional Long Short Term Memory Network

LSTM networks control the flow of information through gating mechanisms, allowing them to selectively store, read, and discard information. These networks are effective in capturing long-term dependencies and, in some ways, alleviating the challenges of gradient vanishing and explosion that recurrent neural networks (RNNs) may face when processing long sequential data [35]. The LSTM network consists of multiple memory cells, each of which contains f_t forget gates, i_t input gates, and o_t output gates:

$$f_t = \sigma(W_f \cdot [h_{t-1}, x_t] + b_f) \tag{1}$$

$$i_t = \sigma(W_i \cdot [h_{t-1}, x_t] + b_i) \tag{2}$$

$$o_t = \sigma(W_o \cdot [h_{t-1}, x_t] + b_o) \tag{3}$$

In Equation (1), σ is the sigmoid activation function, W is the weight matrix, h_{t-1} is the previous moment's hidden state, x_t is the present input, and b is the bias.

While the input gate determines whether the current input data should be retained in the memory cell, the forget gate primarily determines how much of the previous memory should be thrown out. The memory cell determines which information to discard and which to retain for the next time step according to the decisions made by both the forgetting and input gates. The output gate controls the amount of information that is passed from the memory cell to the hidden state, which is then used as the output for the current time step and passed to the next time step or layer. The final output value is calculated by multiplying the output gate's result by the state of the memory cell. However, standard LSTMs can only process data in a unidirectional manner, typically from the beginning to the end of the sequence. This limits their ability to capture dependencies that may span across different time steps, restricting their understanding of the full context within the sequence. To overcome this constraint, the BiLSTM network introduced by Graves et al. [36] utilizes two distinct LSTM layers at each time step: one for processing the sequence in a forward direction (from beginning to end), and the other for processing it in reverse (from end to beginning). Figure 1 illustrates the architecture of the BiLSTM.

The core idea behind BiLSTM is to capture bidirectional dependencies in a sequence by combining the outputs from both the forward and backward LSTM layers. This bidirectional mechanism allows the model to integrate contextual information from both directions, thereby capturing complex dependencies in sequences more comprehensively. It consequently greatly improves the model's comprehension and forecasting capabilities for time-series data. In the joint SOC-SOH estimation task presented in this paper, BiLSTM enables more accurate joint estimation by capturing important temporal dependencies in

the battery discharge process and effectively combining both short-term and long-term features within the battery sequence data.

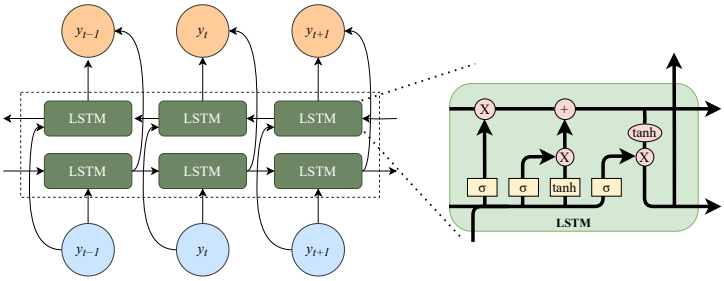

Figure 1. BiLSTM structure diagram.

2.2. Self-Attention Mechanism

SA is widely used in natural language processing and computer vision to capture correlations within sequences [37]. The core idea is to enable the model to process inputs at each time step by considering not only local neighborhood information but also focusing on other parts of the same input sequence. By extending beyond the local scope, this flexibility allows the model to capture global dependencies between elements. Additionally, the SA offers the advantage of not requiring sequential processing of the input sequence; instead, all elements in the sequence can be processed simultaneously. The model can adjust the attention weights dynamically across various time steps, giving greater focus to important steps while disregarding less relevant ones [38]. Figure 2 illustrates the structure of the SA.

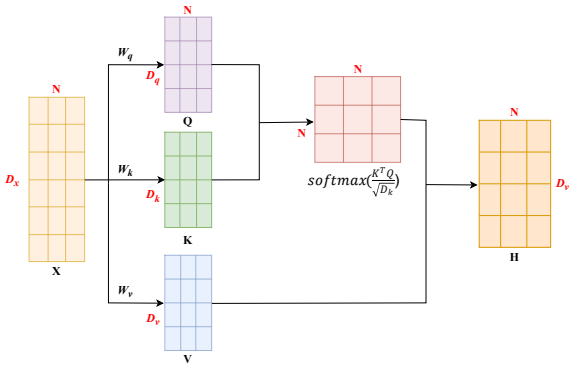

Figure 2. Self-attention structure diagram.

First, the inputs are transformed into three sets of vectors: query (Q), key (K), and value (V). The similarity is then calculated using the dot product between Q and K, followed by the normalization of the similarity scores to obtain the attention weights. Next, these attention weights are applied to the value vectors, and the resulting output is the weighted total of the value vectors:

$$Q = XW_q, K = XW_k, V = XW_v \tag{4}$$

In Equation (4), W_q, W_k and W_v are learnable weight matrices. Following the creation of these vectors, the dot product of Q and K is used to calculate their similarity:

$$Attention(Q, K, V) = softmax(\frac{QK^T}{\sqrt{d_k}})V \tag{5}$$

In Equation (5), d_k is the key's dimension, utilized for scaling the dot product to avoid the issue of vanishing gradients or gradient explosions brought on by excessively high

dot product values. The $softmax$ function normalizes the similarity scores to obtain the attention weights and then performs a weighted summation on each value vector V to obtain the final output:

$$Output = Attention(Q, K, V) \tag{6}$$

2.3. SOC-SOH Joint Estimation Model

This paper proposes the BiLSTM-SA model for joint SOC-SOH estimation in lithium-ion batteries. Although BiLSTM can efficiently deal with time-series data, it still suffers from a certain limitation when faced with long sequences or the task that needs to give different attentions to different parts of the sequences. certain limitations. Through the SA, the joint SOC-SOH model can not only focus on the important time steps in the battery discharge process but also analyze the interactions between different time steps through a globalized perspective. Compared with the traditional sequence modeling method, the incorporation of the SA makes the model more flexible and efficient in dealing with nonlinear and complex time-dependent problems, thus improving the prediction accuracy of SOC and SOH.

In the model design, through its bidirectional processing mechanism, BiLSTM leverages both forward and backward dependencies to efficiently capture the global information in the time-series data. The addition of SA further strengthens the capacity of the model to recognize and extract characteristics from significant time steps. By dynamically modifying the weight allocation to various time steps, SA helps the model in concentrating on the most pertinent data, improving its performance on nonlinear time-series tasks. Figure 3 shows the BiLSTM-SA model structure.

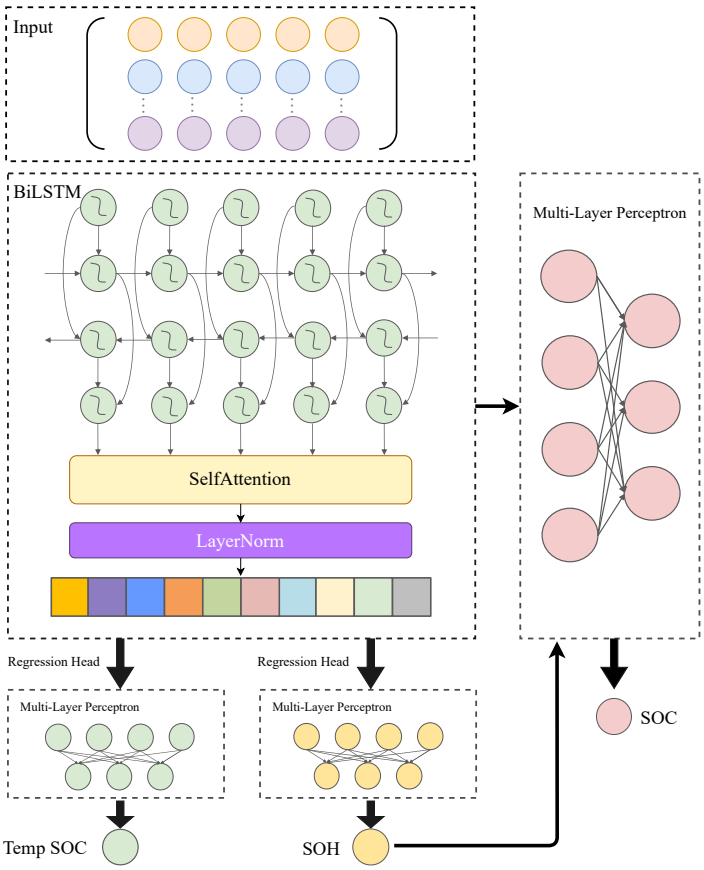

Figure 3. BiLSTM-SA structure diagram.

In the BiLSTM-SA model, the model inputs include voltage, current, temperature, and power, and through the shared BiLSTM layer and SA, it extracts temporal features

during the battery's discharge process. The SA further enhances the model's focus on key time points, increasing the SOC and SOH estimations' accuracy. SOH predictions and provisional SOC values are obtained through two independent fully connected layers, which share the underlying features to capture the coupling between SOC and SOH, despite their separate prediction branches. To refine the SOC prediction, the SOH estimate is introduced as an additional feature, providing more accurate SOC predictions through a new fully connected layer. By incorporating the long-term degradation information from SOH estimation, the shared feature extractor captures the coupling between SOC and SOH more effectively. This shared information strengthens the model's perception of the battery's overall state while raising the stability and precision of the SOC estimation. Figure 4 displays the overall structure of the model.

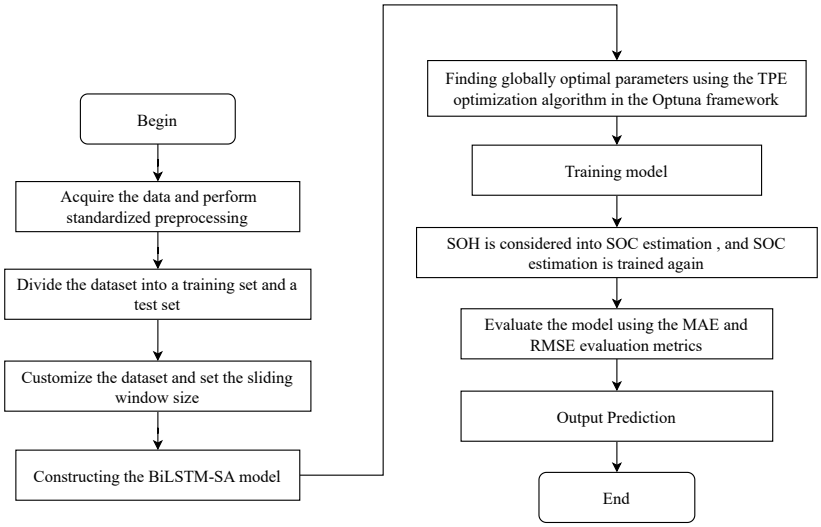

Figure 4. Model's overall flowchart.

The specific implementation procedure for the proposed SOC-SOH joint estimation model for lithium-ion batteries is outlined below.

Step 1: First, the raw data are read, and the sampling frequency is adjusted to 1 Hz to reduce redundancy and increase processing efficiency. Then, the data are normalized to eliminate differences in scale and range of values between variables. The standardization formula is shown in Equation (7):

$$X_{\text{standardized}} = \frac{X - \mu}{\sigma} \tag{7}$$

where X is the raw data value, μ denotes the average of the data, and σ stands for the standard deviation of the data.

Step 2: Split the data into a training set and a testing set based on different driving conditions to ensure that the model can learn and validate under multiple conditions.

Step 3: Load the processed data into the customized dataset class and apply the sliding window approach with a window size of 50. This approach decomposes the discharge cycle into smaller sub-sequences, each representing a specific segment of the cycle.

Step 4: In this step, the joint SOC-SOH estimation modeling is performed using BiLSTM-SA. The model takes voltage, current, temperature, and power data as inputs. These four features are processed through a shared feature extraction layer, which captures common patterns across both SOC and SOH tasks. The model then branches into separate pathways for the joint prediction of SOC and SOH. The predicted SOH is incorporated as a

feature in the SOC prediction, allowing the final SOC estimate to account for the battery's aging process.

Step 5: The joint SOC and SOH estimation model based on BiLSTM-SA is trained using the Adam optimizer. Hyperparameter tuning is conducted using the Optuna framework, which employs the Tree-structured Parzen Estimator method based on Bayesian optimization. The quantity of hidden layer neurons is optimized within the range [10, 100], the count of hidden layers within [1, 5], and the learning rate within $[1 \times 10^{-5}, 1 \times 10^{-1}]$. After optimization, the final values selected are 42 hidden neurons, 4 hidden layers, and a learning rate of 0.001. With this configuration, the model achieves robust SOH estimation, and SOC estimation also shows promising results.

Step 6: SOC-SOH joint estimation for lithium-ion batteries is performed, designing a joint learning model to simultaneously capture sequence-related information pertinent to both SOH and SOC, and obtaining an optimal model for SOH estimation and a provisional SOC model.

Step 7: Consider SOH in the SOC estimation and train the SOC model again.

Step 8: The trained model is utilized for joint SOC-SOH estimation, and the final SOC-SOH predictions are evaluated and analyzed using performance metrics to assess the model's overall effectiveness.

3. Results

3.1. Datasets

This paper uses the LG HG2 battery dataset [39,40] created by Phillip Kollmeyer's team at McMaster University, for experiments focused on electric vehicle applications. The experiments are conducted at six different ambient temperatures: 40 °C, 25 °C, 10 °C, 0 °C, −10 °C, and −20 °C. The battery is charged to 4.2 V at a 1 C rate, followed by a 50 mA cutoff current after each test. The dataset includes standard automotive driving cycles such as US06, HWFET, LA92 and UDDS. US06 simulates high-acceleration EV conditions, HWFET is tested at 60 mph, LA92 simulates urban driving in Los Angeles, and UDDS is suitable for light-duty vehicle driving. Additionally, eight mixed cycles (Mixed 1 to Mixed 8) are created from random combinations of four standard cycles. Data on battery voltage, current, temperature, and consumption are recorded at a 0.1 s sampling rate. In this study, Mixed 1 to Mixed 8 (63%) at −10 °C to 25 °C are used as the training data, while US06, UDDS, LA92, and HWFET (37%) are used for testing.

3.2. Model Evaluation Methodology

Mean absolute error (MAE) and root mean square error (RMSE) are employed as evaluation metrics to assess the precision of BiLSTM-SA for joint SOC-SOH estimation. MAE is a frequently used metric to assess how well regression models predict outcomes. By calculating the mean of these absolute differences, it displays the mean difference in comparison with the expected and actual values, thereby indicating the average error in the model's predictions. The formula for MAE is

$$MAE = \frac{1}{n}\sum_{i=1}^{n}|y_i - \hat{y}_i| \tag{8}$$

In Equation (8), y_i and $\hat{y}_i$ are the actual and estimated values of each time step, respectively, and nnn is the length of the sequence. A smaller MAE value indicates a more accurate model prediction. Since MAE uses the absolute error, it is unaffected by the direction of error and represents the average magnitude of the prediction errors. Additionally, MAE is less sensitive to large deviations, so the overall error is not amplified by a few extreme error points.

RMSE is widely utilized to quantify the difference between predicted and reality values. It is computed through first finding the mean squared error and then taking the square root. The formula for RMSE is

$$RMSE = \sqrt{\frac{1}{n}\sum_{i=1}^{n}(y_i - \hat{y}_i)^2} \tag{9}$$

In Equation (9), y_i is the actual value, $\hat{y}_i$ is the estimated value, and n is the length of the sequence. A more accurate model prediction is indicated by a smaller RMSE value. RMSE gives more weight to larger errors because it squares each error term, allowing it to reflect the overall fluctuation in the model's prediction errors, especially for points with larger errors. This characteristic enables RMSE to highlight the model's performance when dealing with data containing outliers. A thorough assessment of the proposed model's performance in SOH and SOC estimation, covering all aspects of estimation accuracy, is conducted using these two evaluation criteria.

3.3. Experimental Results

To evaluate the suggested joint SOC-SOH estimation method's efficacy, this section systematically conducts experimental validation of the model's performance on the test set. All experiments were conducted using Python 3.11 and PyTorch 2.2.1.

3.3.1. Comparison of SOC Estimates Considering SOH and Without SOH

To capture the influence and coupling relationship of SOH on SOC estimation, we validate the model's performance with and without SOH consideration, analyzing both conditions separately. Table 1 shows the SOC estimation performance with and without SOH inclusion. At −10 °C, the RMSEs for the LA92, UDDS, and US06 cases decrease from 1.32%, 1.72%, and 1.77% to 1.18%, 1.56%, and 1.31%, respectively. This indicates that including SOH in low-temperature environments effectively reduces SOC estimation error. At 0 °C, a similar trend is observed across all four conditions (HWFET, LA92, UDDS, and US06). For instance, the RMSE decreases from 1.85% to 1.33% for the HWFET condition and from 1.49% to 0.94% for the UDDS condition. Under higher-temperature conditions (e.g., 10 °C and 25 °C), the improvement is less pronounced, though SOC estimates still benefit from SOH consideration in some cases. At 10 °C, the RMSE for the HWFET case decreases significantly from 2.45% to 1.13%. However, in other cases, such as US06, the RMSE reduction is smaller. At 25 °C, SOC estimates for the LA92 and UDDS cases are also notably improved with SOH consideration, with the RMSE for the LA92 case reduced from 0.65% to 0.43%.

Overall, the results in Table 1 demonstrate that incorporating SOH information can effectively improve SOC estimation accuracy, with this effect being especially pronounced in low-temperature environments. This finding verifies the coupling relationship between SOH and SOC and suggests that including SOH information in SOC estimation allows for greater capture of the battery's health state, hence improving the estimation accuracy.

To intuitively demonstrate the model's fitting effect when SOH is considered, we compare the estimated SOC curves for the LA92 and US06 conditions at 10 °C and −10 °C, as shown in Figure 5. The figure makes it clear that when SOH information is included in the model, the estimated SOC curve approaches the actual SOC. This result indicates that considering SOH enhances the ability of the model in capturing SOC trends, making the estimation more accurate and stable. This improvement arises because SOH variations are strongly connected to battery aging, temperature, and operating conditions, which directly influence the battery's available capacity and the characteristics of discharge. By incorporating SOH into the SOC estimation process, the model better captures the dynamic

internal state changes of the battery, thus generating SOC estimation curves that align more closely with the actual values. In summary, the comparison results in Figure 5 further validate the key role of SOH in SOC prediction. In addition to increasing the precision of estimating SOC, taking SOH into account increases the model's sensitivity to the battery's health condition, strengthening the estimation results.

Table 1. RMSE evaluation metrics table for SOC estimation with and without SOH under different temperature conditions.

Temperature	Evaluation Method	Standard	Without SOH	With SOH
−10 °C	RMSE (%)	HWFET	1.29	1.43
		LA92	1.32	1.18
		UDDS	1.72	1.56
		US06	1.77	1.31
0 °C	RMSE (%)	HWFET	1.85	1.33
		LA92	1.15	0.81
		UDDS	1.49	0.94
		US06	2.43	1.40
10 °C	RMSE (%)	HWFET	2.45	1.13
		LA92	1.42	1.44
		UDDS	1.18	1.22
		US06	3.11	2.77
25 °C	RMSE (%)	LA92	0.65	0.43
		UDDS	0.92	0.72
		US06	1.16	0.84
Total			1.48	1.20

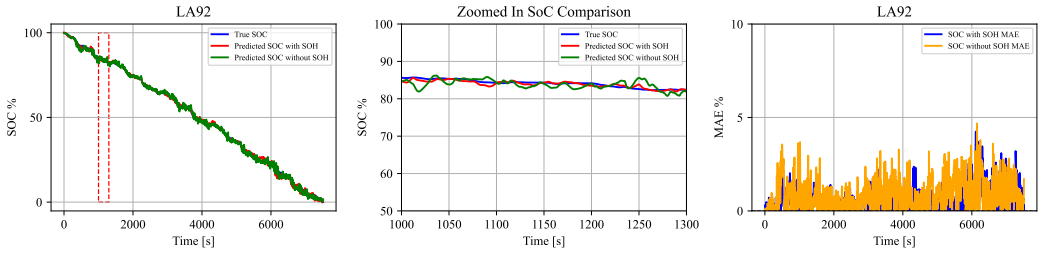

(**a**)

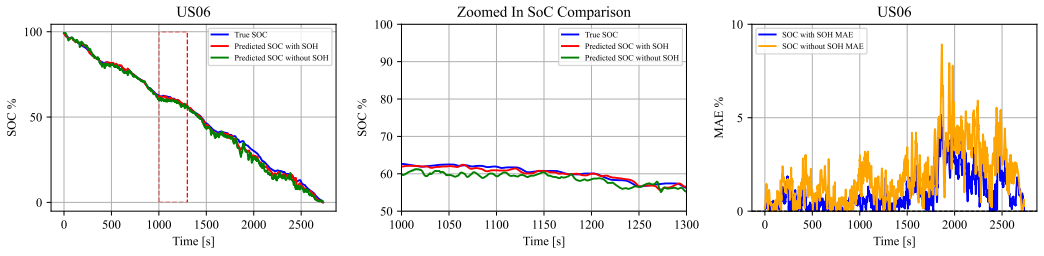

(**b**)

Figure 5. *Cont.*

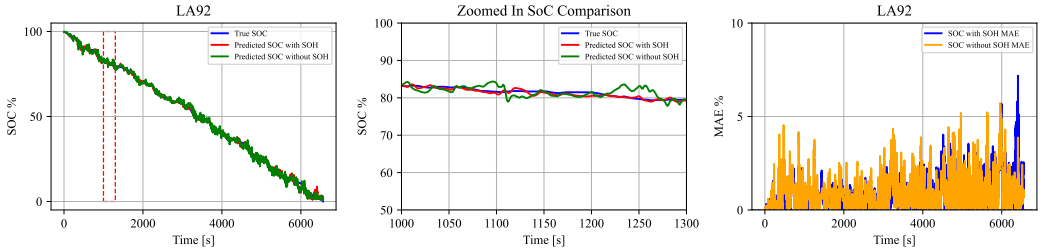

(**c**)

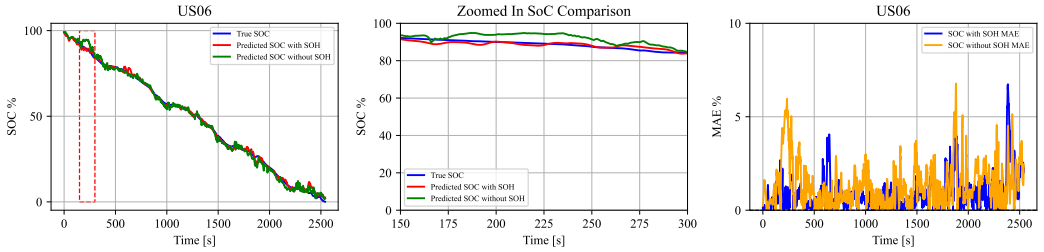

(**d**)

Figure 5. Comparison of SOC estimation curves with and without SOH for LA92 and US06 at 10 °C. and −10 °C. The dashed lines indicate the zoomed-in regions for better clarity. (**a**) SOC estimation of LA92 at 10 °C. (**b**) SOC estimation of US06 at 10 °C. (**c**) SOC estimation of LA92 at −10°C. (**d**) SOC estimation of US06 at −10 °C. The dashed lines indicate the zoomed-in regions for better clarity.

3.3.2. SOC-SOH Estimation at Multiple Temperatures

Table 2 presents the MAE and RMSE values for the joint SOC-SOH estimation of the BiLSTM-SA model under HWFET, LA92, UDDS, and US06 at multi-temperature. The table shows that while prediction accuracy varies slightly with temperature and working conditions, the model overall maintains high accuracy. At −10 °C, the MAE and RMSE for the LA92 are 0.87% and 1.18%, correspondingly, indicating good estimation accuracy, while the RMSE for the US06 case is the lowest at 1.31%. At 0 °C, the MAE and RMSE for the LA92 decrease further to 0.59% and 0.81%, suggesting relatively low prediction error and high robustness for this case. At 10 °C, the MAE for the HWFET case is 0.96%, while the RMSE for the US06 rises to 2.77%, indicating a larger error fluctuation. At 25 °C, the model achieves MAE and RMSE values of 0.34% and 0.43%, with the former representing the smallest error for LA92 across all conditions and temperatures.

Table 2. SOC-SOH estimation experimental results.

Temperature	Standard	RMSE (%)	MAE (%)
−10 °C	HWFET	1.43	1.14
	LA92	1.18	0.87
	UDDS	1.56	1.01
	US06	1.31	0.90
−10 °C	HWFET	1.33	1.01
	LA92	0.81	0.59
	UDDS	0.94	0.67
	US06	1.40	0.99
−10 °C	HWFET	1.13	0.96
	LA92	1.44	1.26
	UDDS	1.22	0.98
	US06	2.77	1.95
25 °C	LA92	0.43	0.34
	UDDS	0.72	0.56
	US06	0.84	0.63
Total		1.20	0.84

Figures 6 and 7 further demonstrate the broad applicability and robustness of the SOC-SOH estimation method. The proposed BiLSTM-SA model requires only one set of network parameters to accurately estimate SOC. Notably, the model performs best at 25 °C. This is because, at room temperature (25 °C), the battery's cycling performance and stability improve, and discharge characteristics are more stable, enhancing the SOC and SOH estimation accuracy.

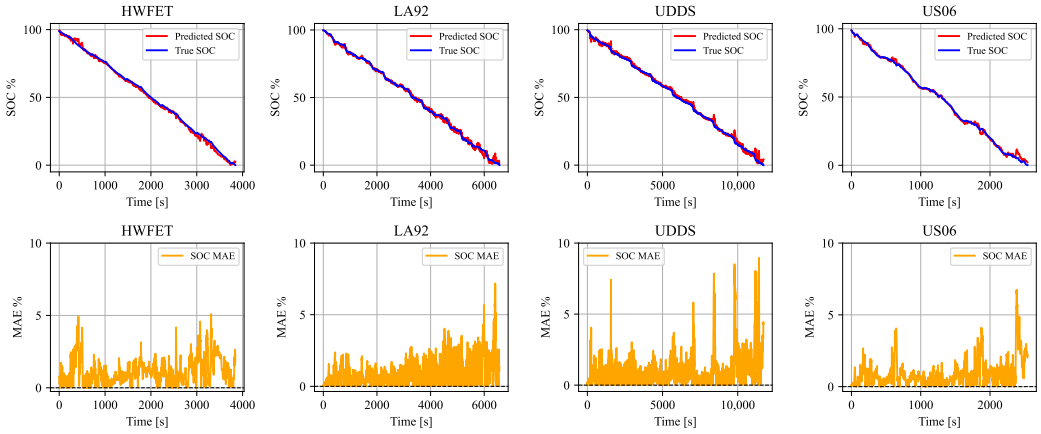

(**a**)

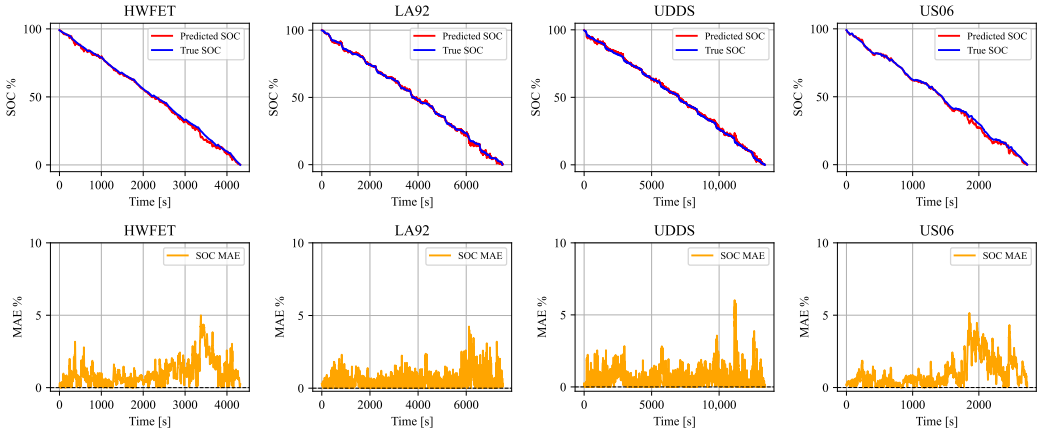

(**b**)

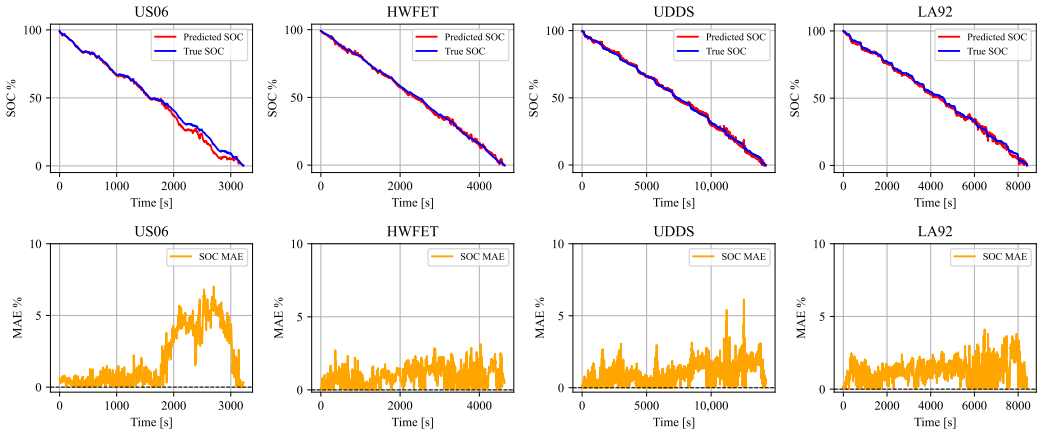

(**c**)

Figure 6. SOC-SOH estimation of HWFET, LA92, UDDS, and US06 at −10 °C, 0 °C and 10 °C. (**a**) SOC estimation at −10 °C. (**b**) SOC estimation at 0 °C. (**c**) SOC estimation at 10 °C.

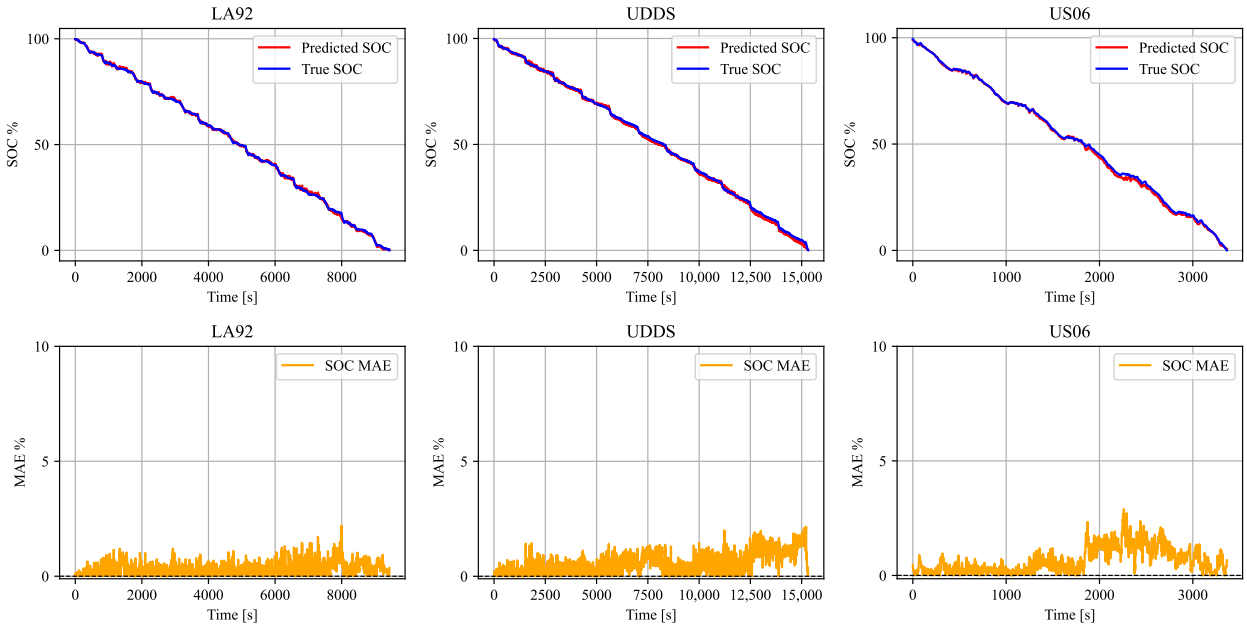

Figure 7. SOC-SOH estimation of LA92, UDDS, and US06 at 25 °C.

3.3.3. Model Comparison

To thoroughly verify the benefits of the BiLSTM-SA model in joint SOC-SOH estimation, we conduct comparative experiments across various models.

Table 3 compares the overall performance of multiple models in the joint SOC-SOH estimation. The BiLSTM-SA model outperforms all other models, with an MAE of 0.84% and an RMSE of 1.20%. This indicates that the BiLSTM-SA model effectively reduces error, resulting in higher precision and improved reliability in the SOC-SOH estimation. The GRU and BiLSTM-MHA models also perform well, with MAEs of 0.84% and 0.87% and RMSEs of 1.23% and 1.26%, respectively, being slightly inferior to BiLSTM-SA. The RNN model shows relatively large errors, with an MAE of 1.19% and an RMSE of 1.63%. The LSTM and BiLSTM models improve compared to the RNN, with MAE values of 0.97% and 0.96% and RMSE values of 1.35% and 1.34%, respectively, though they still lag behind the BiLSTM-SA. The TCN-LSTM and LSTM-SA models show the poorest results, with MAEs of 1.53% and 1.37% and RMSEs of 2.15% and 1.85%. Overall, the SA in BiLSTM allows the BiLSTM-SA model to better capture key features, significantly improving estimation accuracy. The findings indicate that the BiLSTM-SA model with SA has a clear performance advantage in joint SOC-SOH estimation, providing excellent accuracy and reliability. This further validates the effectiveness of SA in complex battery state estimation, enabling the BiLSTM-SA model to better meet the prediction needs under multi-temperature conditions.

Compared with other models, BiLSTM-SA demonstrates stronger adaptability and generalization in complex tasks, especially in scenarios where battery performance fluctuates with time, temperature, and workload. Figures 8 and 9 show the comparison results for LA92 and UDDS at 25 °C, 0 °C, and −10 °C. The figure reveals that the curve fitting of BiLSTM-SA surpasses that of the other models, demonstrating its higher prediction accuracy and stronger reliability.

Table 3. Comparison experiment results.

Model	MAE (%)	RMSE (%)
RNN	1.19	1.63
LSTM	0.97	1.35
BiLSTM	0.96	1.34
GRU	0.91	1.29
BiGRU	0.98	1.34
TCN-LSTM	1.53	2.15
CNN-LSTM	1.29	1.72
LSTM-SA	1.37	1.85
GRU-SA	0.94	1.32
BiLSTM-CA	0.93	1.34
BiLSTM-MHA	0.87	1.26
BiLSTM-SA	**0.84**	**1.20**

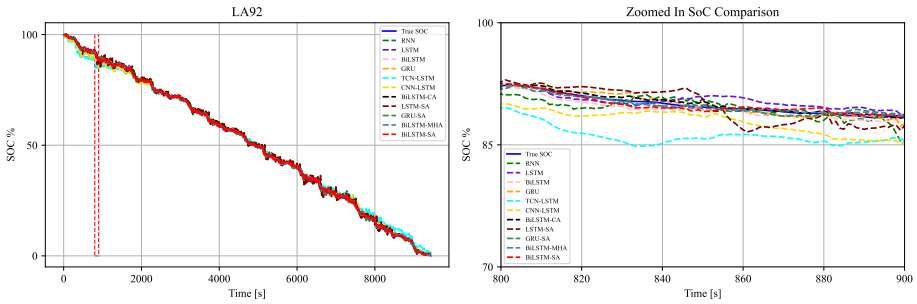

(**a**)

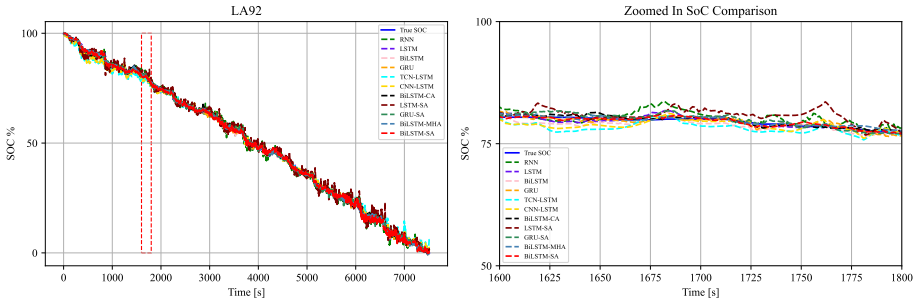

(**b**)

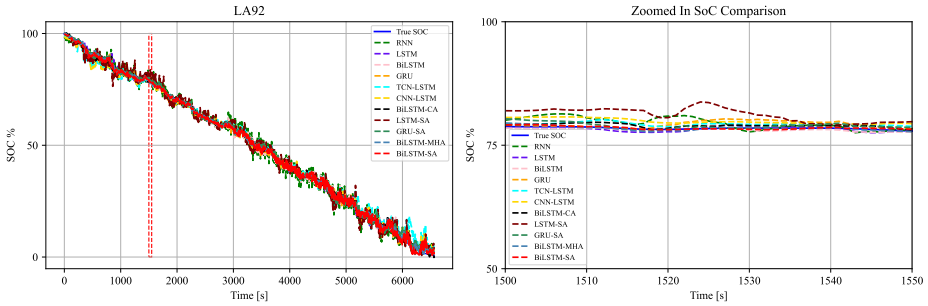

(**c**)

Figure 8. SOC-SOH estimation models for LA92 are compared at temperatures of 25 °C, 0 °C, and −10 °C. The dashed lines indicate the zoomed-in regions for better clarity. (**a**) SOC estimation of LA92 at 25 °C. (**b**) SOC estimation of LA92 at 0 °C. (**c**) SOC estimation of LA92 at −10 °C.

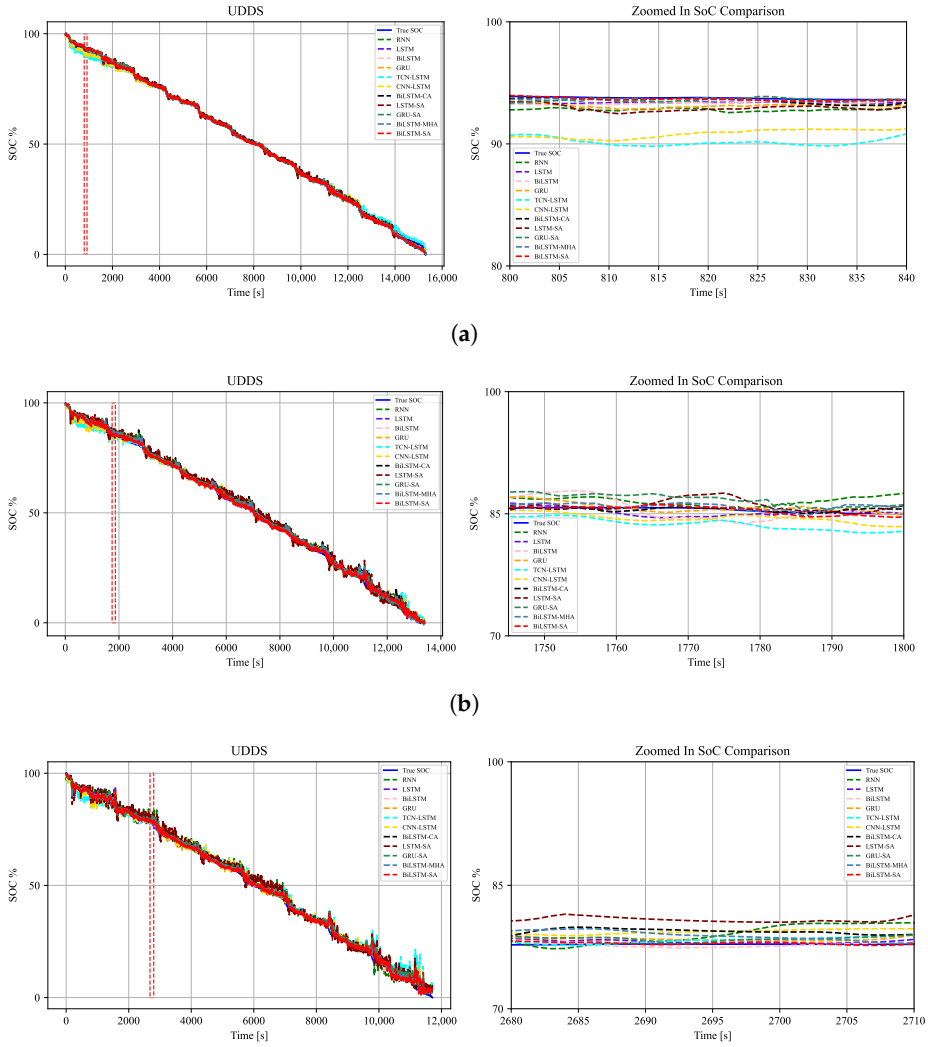

Figure 9. SOC-SOH estimation models for UDDS are compared at temperatures of 25 °C, 0 °C, and −10 °C. The dashed lines indicate the zoomed-in regions for better clarity. (**a**) SOC estimation of UDDS at 25 °C. (**b**) SOC estimation of UDDS at 0 °C. (**c**) SOC estimation of UDDS at −10 °C.

4. Conclusions

In this paper, BiLSTM-SA models are trained on data at −10 °C, 0 °C, 10 °C, and 25 °C temperatures and tested on the HWFET, LA92, UDDS, and US06 datasets. Comparative analysis shows the clear advantages of the BiLSTM-SA model over traditional BiLSTM, LSTM, and RNN models in SOC-SOH estimation. The BiLSTM-SA model captures complex dependencies in the sequence data, and the SA enables the model to focus on key information, significantly reducing SOC-SOH prediction errors. In terms of key metrics like RMSE and MAE, the BiLSTM-SA model outperforms other models, further validating its preciseness and robustness in joint SOC-SOH estimation. The model performs well on a dataset covering various temperatures and operating conditions (e.g., different driving cycles). This provides reliable technical support and a solid theoretical foundation for applying BMS in complex situations in the real world. Future studies could concentrate on multi-state joint estimation, exploring more sophisticated network architectures and optimization algorithms to enhance the versatility of the model and effectiveness in a broader range of situations. Additionally, combining feature engineering with data enhancement strategies may further boost the model's predictive capabilities under more challenging conditions, driving continued advancements and the wider adoption of BMS solutions.

Author Contributions: Conceptualization, L.W. and C.C.; methodology, L.W. and Z.L.; software, L.W. and Z.L.; validation, L.W., Z.L. and Z.C.; formal analysis, L.W. and H.L.; investigation, L.W., Z.C. and H.L.; resources, L.W.; data curation, L.W. and Z.L.; writing—original draft preparation, L.W.; writing—review and editing, L.W. and C.C.; visualization, L.W.; supervision, C.C.; project administration, L.W.; funding acquisition, C.C. All authors have read and agreed to the published version of the manuscript.

Funding: This work was supported by the Science and Technology Innovation Talent Fund of Sichuan Provincial Department of Science and Technology (No. 2024JDRC0013), and the Scientific Research and Innovation Team Program of Sichuan University of Technology (No. SUSE652A006). This study was supported by the computational support provided by the High-Performance Computing Center, Sichuan University of Science and Engineering.

Data Availability Statement: Data are contained within the article.

Conflicts of Interest: The authors declare no conflicts of interest.

References

1. Su, M.; Huang, G.; Wang, S.; Wang, Y.; Wang, H. High safety separators for rechargeable lithium batteries. *Sci. China Chem.* **2021**, *64*, 1131–1156. [CrossRef]
2. Alsuwian, T.; Ansari, S.; Zainuri, M.A.A.M.; Ayob, A.; Hussain, A.; Lipu, M.H.; Alhawari, A.R.; Almawgani, A.; Almasabi, S.; Hindi, A.T. A Review of Expert Hybrid and Co-Estimation Techniques for SOH and RUL Estimation in Battery Management System with Electric Vehicle Application. *Expert Syst. Appl.* **2024**, *246*, 123123. [CrossRef]
3. Lipu, M.H.; Ansari, S.; Miah, M.S.; Meraj, S.T.; Hasan, K.; Shihavuddin, A.; Hannan, M.; Muttaqi, K.M.; Hussain, A. Deep learning enabled state of charge, state of health and remaining useful life estimation for smart battery management system: Methods, implementations, issues and prospects. *J. Energy Storage* **2022**, *55*, 105752. [CrossRef]
4. Kumar, R.R.; Bharatiraja, C.; Udhayakumar, K.; Devakirubakaran, S.; Sekar, S.; Mihet-Popa, L. Advances in batteries, battery modeling, battery management system, battery thermal management, SOC, SOH, and charge/discharge characteristics in EV applications. *IEEE Access* **2023**, *11*, 105761–105809. [CrossRef]
5. Nyamathulla, S.; Dhanamjayulu, C. A review of battery energy storage systems and advanced battery management system for different applications: Challenges and recommendations. *J. Energy Storage* **2024**, *86*, 111179. [CrossRef]
6. Zeng, J.; Liu, S. Research on aging mechanism and state of health prediction in lithium batteries. *J. Energy Storage* **2023**, *72*, 108274. [CrossRef]
7. Zhang, M.; Yang, D.; Du, J.; Sun, H.; Li, L.; Wang, L.; Wang, K. A review of SOH prediction of Li-ion batteries based on data-driven algorithms. *Energies* **2023**, *16*, 3167. [CrossRef]
8. Espedal, I.B.; Jinasena, A.; Burheim, O.S.; Lamb, J.J. Current trends for state-of-charge (SoC) estimation in lithium-ion battery electric vehicles. *Energies* **2021**, *14*, 3284. [CrossRef]
9. Zhang, Q.; Wang, D.; Yang, B.; Dong, H.; Zhu, C.; Hao, Z. An electrochemical impedance model of lithium-ion battery for electric vehicle application. *J. Energy Storage* **2022**, *50*, 104182. [CrossRef]
10. Gismero, A.; Schaltz, E.; Stroe, D.I. Recursive state of charge and state of health estimation method for lithium-ion batteries based on coulomb counting and open circuit voltage. *Energies* **2020**, *13*, 1811. [CrossRef]
11. Movassagh, K.; Raihan, A.; Balasingam, B.; Pattipati, K. A critical look at coulomb counting approach for state of charge estimation in batteries. *Energies* **2021**, *14*, 4074. [CrossRef]
12. Dini, P.; Colicelli, A.; Saponara, S. Review on modeling and SOC/SOH estimation of batteries for automotive applications. *Batteries* **2024**, *10*, 34. [CrossRef]
13. Yang, F.; Xing, Y.; Wang, D.; Tsui, K.L. A comparative study of three model-based algorithms for estimating state-of-charge of lithium-ion batteries under a new combined dynamic loading profile. *Appl. Energy* **2016**, *164*, 387–399. [CrossRef]
14. Hosseininasab, S.; Lin, C.; Pischinger, S.; Stapelbroek, M.; Vagnoni, G. State-of-health estimation of lithium-ion batteries for electrified vehicles using a reduced-order electrochemical model. *J. Energy Storage* **2022**, *52*, 104684. [CrossRef]
15. Demirci, O.; Taskin, S.; Schaltz, E.; Demirci, B.A. Review of battery state estimation methods for electric vehicles—Part II: SOH estimation. *J. Energy Storage* **2024**, *96*, 112703. [CrossRef]
16. How, D.N.; Hannan, M.; Lipu, M.H.; Ker, P.J. State of charge estimation for lithium-ion batteries using model-based and data-driven methods: A review. *IEEE Access* **2019**, *7*, 136116–136136. [CrossRef]
17. Kouhestani, H.S.; Liu, L.; Wang, R.; Chandra, A. Data-driven prognosis of failure detection and prediction of lithium-ion batteries. *J. Energy Storage* **2023**, *70*, 108045. [CrossRef]

18. Demirci, O.; Taskin, S.; Schaltz, E.; Demirci, B.A. Review of battery state estimation methods for electric vehicles—Part I: SOC estimation. *J. Energy Storage* **2024**, *87*, 111435. [CrossRef]
19. Kurucan, M.; Özbaltan, M.; Yetgin, Z.; Alkaya, A. Applications of artificial neural network based battery management systems: A literature review. *Renew. Sustain. Energy Rev.* **2024**, *192*, 114262. [CrossRef]
20. Ren, Z.; Du, C. A review of machine learning state-of-charge and state-of-health estimation algorithms for lithium-ion batteries. *Energy Rep.* **2023**, *9*, 2993–3021. [CrossRef]
21. Chen, C.; Li, Z.; Wei, J. Estimation of Lithium-Ion Battery State of Charge Based on Genetic Algorithm Support Vector Regression under Multiple Temperatures. *Electronics* **2023**, *12*, 4433. [CrossRef]
22. Li, H.; Chen, C.; Wei, J.; Chen, Z.; Lei, G.; Wu, L. State of Health (SOH) Estimation of Lithium-Ion Batteries Based on ABC-BiGRU. *Electronics* **2024**, *13*, 1675. [CrossRef]
23. Bian, C.; He, H.; Yang, S. Stacked bidirectional long short-term memory networks for state-of-charge estimation of lithium-ion batteries. *Energy* **2020**, *191*, 116538. [CrossRef]
24. Eddahech, A.; Briat, O.; Vinassa, J.M. Adaptive voltage estimation for EV Li-ion cell based on artificial neural networks state-of-charge meter. In Proceedings of the 2012 IEEE International Symposium on Industrial Electronics, Hangzhou, China, 28–31 May 2012; IEEE: Piscataway, NJ, USA, 2012; pp. 1318–1324. [CrossRef]
25. Yang, F.; Li, W.; Li, C.; Miao, Q. State-of-charge estimation of lithium-ion batteries based on gated recurrent neural network. *Energy* **2019**, *175*, 66–75. [CrossRef]
26. Zhang, X.; Liu, X.; Li, J. A Novel Method for Battery SOC Estimation Based on Slime Mould Algorithm Optimizing Neural Network under the Condition of Low Battery SOC Value. *Electronics* **2023**, *12*, 3924. [CrossRef]
27. Zhong, C.M.; Li, G.Y.; Zheng, X.; Su, Y.H.; Zhou, B.H.; Lu, Y.J.; Chen, Z.; Guo, W.J. Supervision and performance optimization of rechargeable battery SoC based on lightweight neural network. *J. Energy Storage* **2024**, *99*, 113374. [CrossRef]
28. Park, M.S.; Lee, J.k.; Kim, B.W. SOH estimation of Li-ion battery using discrete wavelet transform and long short-term memory neural network. *Appl. Sci.* **2022**, *12*, 3996. [CrossRef]
29. Qian, C.; Xu, B.; Xia, Q.; Ren, Y.; Sun, B.; Wang, Z. SOH prediction for Lithium-Ion batteries by using historical state and future load information with an AM-seq2seq model. *Appl. Energy* **2023**, *336*, 120793. [CrossRef]
30. Yang, B.; Wang, Y.; Zhan, Y. Lithium battery state-of-charge estimation based on a Bayesian optimization bidirectional long short-term memory neural network. *Energies* **2022**, *15*, 4670. [CrossRef]
31. Van, C.N.; Quang, D.T. Estimation of SoH and internal resistances of Lithium ion battery based on LSTM network. *Int. J. Electrochem. Sci.* **2023**, *18*, 100166. [CrossRef]
32. Lai, X.; Yuan, M.; Tang, X.; Yao, Y.; Weng, J.; Gao, F.; Ma, W.; Zheng, Y. Co-estimation of state-of-charge and state-of-health for lithium-ion batteries considering temperature and ageing. *Energies* **2022**, *15*, 7416. [CrossRef]
33. Wu, T.; Liu, S.; Wang, Z.; Huang, Y. SOC and SOH joint estimation of lithium-ion battery based on improved particle filter algorithm. *J. Electr. Eng. Technol.* **2022**, *17*, 307–317. [CrossRef]
34. Fang, X.; Xu, M.; Fan, Y. SOC-SOH Estimation and Balance Control Based on Event-Triggered Distributed Optimal Kalman Consensus Filter. *Energies* **2024**, *17*, 639. [CrossRef]
35. Kawakami, K. Supervised Sequence Labelling with Recurrent Neural Networks. Ph.D. Thesis, Technical University of Munich, Munich, Germany, 2008. [CrossRef]
36. Graves, A.; Schmidhuber, J. Framewise phoneme classification with bidirectional LSTM and other neural network architectures. *Neural Netw.* **2005**, *18*, 602–610. [CrossRef]
37. Li, Q.; Yao, N.; Zhao, J.; Zhang, Y. Self attention mechanism of bidirectional information enhancement. *Appl. Intell.* **2022**, *52*, 2530–2538. https://doi.org/10.1007/s10489-021-02492-2.
38. Chen, J.; Zhang, C.; Chen, C.; Lu, C.; Xuan, D. State-of-charge estimation of lithium-ion batteries using convolutional neural network with self-attention mechanism. *J. Electrochem. Energy Convers. Storage* **2023**, *20*, 031010. [CrossRef] [PubMed]
39. Vidal, C.; Kollmeyer, P.; Naguib, M.; Malysz, P.; Gross, O.; Emadi, A. Robust xev battery state-of-charge estimator design using a feedforward deep neural network. *SAE Int. J. Adv. Curr. Pract. Mobil.* **2020**, *2*, 2872–2880. [CrossRef]
40. Kollmeyer, P.; Vidal, C.; Naguib, M.; Skells, M. LG 18650HG2 Li-ion Battery Data and Example Deep Neural Network xEV SOC Estimator Script. *Mendeley Data* **2020**, *3*, 2020. [CrossRef]